Research and Calculation of the Belt Cutting Process of 23mm Cased Telescoped Ammunition by Numerical Method

Duong Hai Son [1], Nguyen Thai Dung[1], Hoang van Dang[1], Vu Duong [2*],

[1]Le Quy Don Technical University

[2]Duy Tan University

Abstract: This paper studies the process of the belt cutting of the cased telescoped ammunition, builds a model that simulates the belt cutting process of a 23mm Cased Telescoped Ammunition by using numerical method with the ANSYS AUTODYN software tool. Apply numerical method to calculate the process of cutting the guide belt. From there, evaluate the influence of projectile structural parameters such as structure and material on the belt cutting process of the 23mm Cased Telescoped Ammunition. The test results show that the simulation operation calculation results reach the required accuracy.

Keywords: Belt cutting, Cased Telescoped Ammunition, numerical method

1. Introduction

The physical processes that occur during the cutting of the guide belt have an important effect on the ballistic parameters of the preliminary period as well as the entire firing process [1, 3]. However, at present, there is not much research on the cutting process of the guide belt to have an overview of the cutting process of the guide belt and its influence on the parameters of the shot, especially for 23mm cased telescoped ammunition.

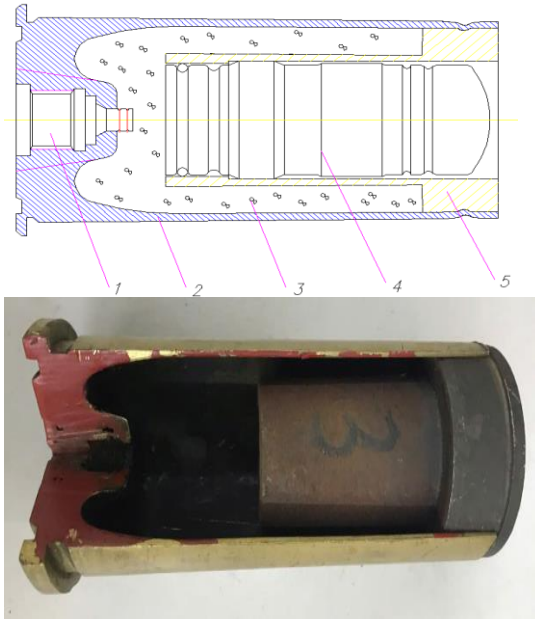

Figure 1. Structure of 23 mm Case Telescoped Ammunitions

1. Primer; 2. Case; 3. Propellant Grain; 4. Projectile; 5. Control tube.

The problem of cutting the guide belt in particular and the problem of metal forming deformation in general are very complicated due to the interaction between the barrel, the projectile body and the guide belt, which makes the guide belt after deformation have a complex shape [2, 5, 6, 7, 8]. Because the problem of cutting the guide belt is very complicated, therefore, the method of modeling and numerical simulation is considered as an effective method to study and optimize the parameters of the guide belt in the process of design and manufacture [9, 11, 14]. Numerical simulation of the guide belt cutting problem to approach the real belt cutting process is carried out by using the finite element method and the numerical simulation method with the help of computers and the applying algorithms in the multi-objective problem. From there, it is possible to reduce the time and cost of the trial manufacturing process.

The firing process is a fast and complex thermodynamic process, staring from the moment the propellant ignites and ending when the projectile flies out of the barrel. The burning propellant will create a very large amount of gas, at the same time the temperature increases suddenly (up to 2,500°C) and the pressure increases very quickly. When the pressure reaches a certain value (called the bullet ejection pressure)

[1, 3], the projectile starts to move. When the propellant burns out, the projectile receives additional kinetic energy due to the free expansion of the high-temperature gas[1,3,19]. The theoretical bullet velocity will be the largest at the muzzle cross-section, but when the projectile flies out of the barrel, the gas overflows and expands, acting on the bottom of the projectile, increasing the projectile velocity slightly. Thus, when the projectile moves in the barrel, its velocity continuously increases and reaches its maximum value at a position about (30÷40)d from the muzzle (d is the barrel diameter).

2.FACTORS AFFECTING THE BELT CUTTING PROCESS OF A 23MM CASED TELESCOPED AMMUNITION

2.1. Influence of ballistic parameters

The effect of the ballistic parameters is related to the cutting process of the guide belt into the barrel groove and the belt cutting resistance force is presented in [3, 12, 13]. In order to win the belt cutting resistance force, the gas must perform additional work A_P ;

$$A_P = \int_{l_H}^{l_\phi} F_{Bp} dl$$

Here: l_ϕ - the guide belt width; l_H - the free distance of projectiles; l_ϕ F_{Bp} - belt cutting resistance force into the barrel groove.

Due to the projectile is axially symmetrical, when taking into account the coefficient of friction, the belt cutting resistance force into the barrel groove can be written

$$F_{Bp} = \int_0^{S_k} \sigma_k (\sin\alpha_k + \mu \cos\alpha_k) dS_k$$

Here S_k - the contact surface area; σ_k - normal stress; μ - the coefficient of friction between barrel wall and guide belt; α_k - the angle between barrel axis and tangent to barrel taper. Note that the coefficient of friction decreases with increasing relative speed of the contact surfaces. For a copper belt, this dependence can be given by the experiment formula

$$v = \mu_0 \frac{1+0,07.v}{1+0,18.v} = \mu_0 f_\mu(v)$$

Where: v - velocity, m/s; μ0 - coefficient of static friction (when v ≈ 0,0003m/s).

The experimental study of belt cutting resistance force under static conditions shows that the value μ0 of the copper belt and the new barrel without lubricant on the surface of the barrel can be taken as 0.093 with conical contact (plastic friction), and 0.2 in the cylindrical part of the barrel (elastic friction).

Along with the energy loss of the gas occurs the pulse loss of the gas pressure I_P to overcome the belt cutting resistance force P :

$$I_P = \int_{t_H}^{t_\phi} P dt$$

Table 1 cites the values of attack A_P and pulse I_P , and at the same time evaluates them in some weapons.

Table 1 shows that the work of belt cutting resistance force is about ten percent of the projectile kinetic energy at the end of the ejection period (E_Φ) and only about one thousandth of the kinetic energy of the muzzle (E_D) (except for infantry guns); the loss pulse of the gas pressure is a few percent of the total pulse of the pressure.

Table 1. Characteristics of losses during the projectile ejection period

Type of ammunition	v_0 m/s	A_P	A_P/E_D(%)	A_P/E_Φ (%)	I_P	I_P/I_D(%)
AKM	715	0,038	1,87	31,5	4,0	4,0
23 mm gun	980	0,156	0,17	15,5	5,0	0,9
D-30 gun	690	7,73	0,15	14,6	5,9	2,4

M-46 gun	930	47,85	0,32	79,2	74,8	3,9
D-20 gun	655	13,90	0,15	14,4	30,7	1,6

For a long time, the effect of the belt cutting process on the value of the initial velocity of the projectile has been explained only with work A_P. However, it is neither the only nor the main factor. The muzzle velocity is directly related to the pulse loss I_D of pressure:

$$v_d = \frac{s}{\varphi q}(I_D^{'} - I_P)$$

In which $I_D^{'}$ - the active pulse of the gas pressure,

$$I_D^{'} = \int_{t_0^{'}}^{t_D} p dt = I_D - I_0$$ ($t_0^{'}$ - duration of static combustion period).

The value I_P for the same belt cutting curve ($P_{cp} = \text{const}$) will depend mainly on the belt cutting time Δt_{Bp}: $I_P = P_{cp}.\Delta t_{Bp}$. So, there appears a more important factor - pulse loss of pressure I_P. It explains the small effect of the belt cutting process on the initial velocity value (when there is free movement of the projectile) due to the increase in the average belt cutting speed and the decrease in the value Δt_{Bp}: $\Delta t_{Bp} = l_{Bp} / \bar{v}_{Bp}$.

Another factor is the amount of propellant burned during the projectile ejection period:

$$\Psi_\Phi = æ \frac{I_\Phi}{I_k}\left(1 + \lambda \frac{I_\Phi}{I_k}\right)$$ or the pulse value of the gas pressure at the end of the projectile ejection period I_Φ. Along with the increase in relative mass of the burned propellant, Ψ_Φ the gas pressure will increase:

$$p_\Phi = \frac{f_\omega}{s}.\frac{\Psi - v_\Phi / v_{np} - (\theta / f\omega)A_P}{l_\Phi + l_{\Psi_\Phi}}$$

and the intensity of its subsequent change :

$$(\frac{dp}{dt})_\Phi \approx p_\Phi \frac{æf\omega}{(\mathrm{W}_0 - \omega/\delta)I_k}$$

This leads to an increase in the pulse of the gas and the muzzle velocity of the projectile. The influence of the latter factor is smaller with thinner and faster burning propellant, which explains why the phenomenon of ejection is not used in mortars. When the propellant burns instantly, the maximum pressure value will not depend on the projectile ejection. When evaluating the influence of the ballistic parameters at the projectile ejection period, it is necessary to first consider the pulse loss I_P and the and the increment of the active pulse $\Delta I_D^{'}$.

In the most general form it can be stated that the influence of the ballistic parameters at the projectile ejection period is determined by the belt cutting curve (belt structure, barrel leading part), cutting conditions (cutting speed, barrel wear and lubrication, etc.) and stuffing parameters (propellant characteristics, combustion chamber volume, etc.).

To quantitatively evaluate the influence of propellant characteristics during the projectile ejection period, the projectile ejection pressure parameter will be used.

2.2. Influence of the projectile ejection system structure

The preliminary period involves the loading and guiding of the projectile in the barrel. The set of elements to carry out the ejection of the projectile is called the projectile ejection system. It includes the connecting part, the barrel guide and the projectile guide and the projectile chamber.

The barrel is divided into the combustion chamber and the guide section by a cross section located at the beginning of the spiral groove or at the end of the smooth cylinder. The combustion chamber is transferred to the guide section by one or two transition cones, which ensure the retention of the projectile with separate - loading ammunitiong and facilitate the cutting of the belt. Usually, the main transition cone is at the beginning of the spiral groove and then there is a smooth cone, in

some guns on the cone there is a groove. The taper of the transition cone is within the limits of 1/10÷1/20. The cone angle α_k when separate - loading is smaller than when instantly-loading, because it is necessary to ensure reliable retention of the projectile [3].

The force required to pull out the projectile F_r after it is held in the smooth cone is determined by the expression:

$$F_r = k_F \pi d \sigma_\tau \sin\alpha_k \left(\frac{\mu}{tg\alpha_k} - 1\right) l_{Bp}$$

In which: k_F - is the coefficient taking into account the characteristics of the stress state of the belt, $k_F \approx 1$.

Belt cutting distance l_{Bp} determined from the kinetic energy balance of the projectole at the time of cutting and the work of belt cutting resistance:

$$\frac{q v_{Bp}^2}{2} = \int_0^{l_{Bp}} F_{Bp} d_l = \frac{1}{2} F_{Bp}^{\max} l_{Bp}$$

From there: $l_{Bp} = \dfrac{q v_{Bp}^2}{F_{Bp}^{\max}}$, where: $F_{Bp}^{\max}$ - the maximum value of belt cutting resistance

$$F_{Bp}^{\max} = k_F \pi d \sigma_\tau \sin\alpha_k \left(\frac{\mu}{tg\alpha_k} + 1\right) l_{Bp}$$

If knowing the pull out force of the projectile will allow determining the value of $F_{Bp}^{\max}$

$$F_{Bp}^{\max} = \frac{\dfrac{\mu}{tg\alpha_k} + 1}{\dfrac{\mu}{tg\alpha_k} - 1} F_r$$

The guide part of the barrel may be smooth or grooved, to center the projectile, orient its flight in space and transmit rotational motion. The rifling grooves are characterized by the angle of inclination to the barrel α_{H} or the relative length of the twist $\eta = \dfrac{\pi}{tg\alpha_H}$.

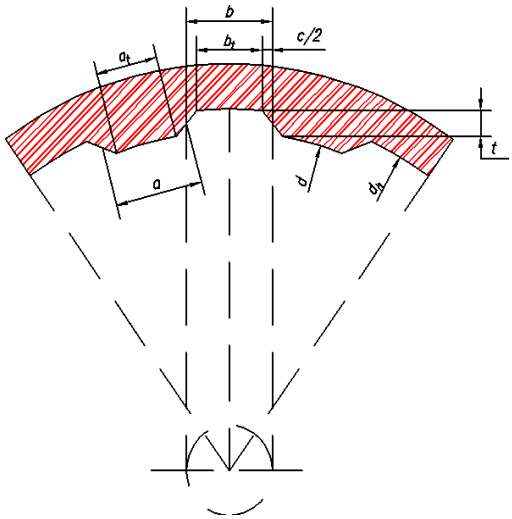

Figure 2. Cross section of barrel with rifling groove

The belt cutting takes place with a constant or increasing slope. The cut profile shape can be rectangular or trapezoidal (fig. 2) and is characterized by geometric dimensions:cutting depth t, width of cutting bottom b (b_τ), width of cutting slice $a(a_\tau)$. In case of a trapezoidal cutting section with inclined edge $c = (b_\tau - a_\tau)$, then the conversion parameter are included: $a' = a_\tau + c$, $b' = b_\tau + c$. The cutting depth usually equal to (1÷2)% of the caliber. The number of grooves n_H is determined by the expression

$$n_H = \frac{\pi d}{a + b}$$

In infantry guns η_H = 4, η_H in artillery is within the range of 12 to 88. The cutting parameter affects the translational movement of the bullet through the cross-sectional area of the barrel.

$$s = \frac{\pi d^2}{4} + n_H t b = \left(\frac{\pi}{4} + n_H \frac{t}{d}\frac{b}{d}\right) d^2 = k_s d^2$$

The coefficient for taking into account the influence of the rifling groove is one of the

ballistic parameters: $k_s = \frac{\pi}{4} + n_H \frac{t}{d}\frac{b}{d}$ when there are no rifling groove parameters can be taken $k_s = 0,79$ as witht a smooth barrels, $k_s = 0,81$ when the rifling groove depth is 1% and $k_s = 0,83$ when the depth of the rifling groove is 2%.

In some cases, when the guide part of the barrel does not change the cross-sectional area is will be replaced by a smooth barrel with a converted diameter d_{qd}: $d_{qd} = \sqrt{\frac{4s}{\pi}} = \sqrt{\frac{4k_s}{\pi}}d$.

The guide part of the projectile is used to center the projectile, transmit it to rotation, and at the same time seal the gas and ensure the retention of the bullet. It includes guide belts and centering belts located on the projectile. The centering belt is the cylindrical surface in contact with the surface of the barrel. To ensure easy loading of the projectile into the barrel, the diameter of the cylindrical surface of the centering belt must be smaller than the caliber of the barrel from 0.10÷ to 0.25mm.

The guide elements need to have ridges, these ridges will be led into the rifling groove and when the projectile moves forword, it will create an angular velocity for projectile ω_{CH}

$$\omega_{CH} = \frac{2tg\alpha_k}{d}v = \frac{2\pi}{\eta}v$$

The guiding elements can be available or created at the first stage of the projectile's movement. In the first case, the guiding elements are manùactured in the form of pins, plates, grooves on the projectile or on the centering elements. In the second case, the guiding elements are made of plastic materials in the form of shells, belts, etc… on the projectile or on the centering element. Currently, to guide projectiles in artillery, one or two guiding belts (sometimes edges) are often used, while in the firearms, they are guided by the projectile body, in which case the diameter d_o of the projectile body is larger than the diameter of the barrel at the bottom of the rifling groove (d_H). Half the diffrence in diameters are called the projectile ejection belt: $\delta_\Phi = \frac{d_0 - d_H}{2}$. (the thickness of the belt).

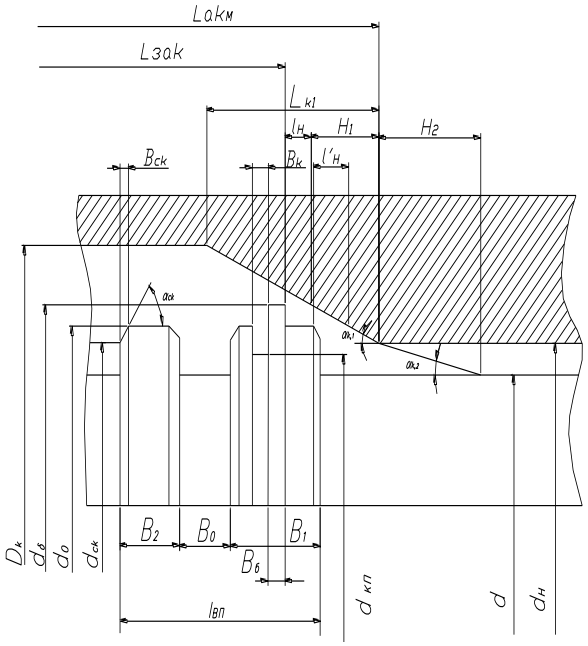

Figure 3. Model of the projectile guide belt in the barrel

Guide belts are usually made of copper alloys (brass, MH95-5), low-carbon steel, ceramic steel, plastic, brass, and plated steel. Guide belts are usually mounted on the projectile body or on the centering belt with swallow-tail grooves by compression or welding, gluing. In addition to guiding the projectile, the guide belts also ensure centering and sealing the gas.

The guide belt is characterized by geometric and mechanical parameters, as well as its location on the projectile body. The location of the guide belt depends on the thickness of the projectile body wall, the distance between the first belt (in the direction of movement) and the second belt is B_0 (Figure 3), the length from the bottom of the barrel to the cross-section of the projectile where the guide belt begins to cut when it meets the transition cone is L_{SD} and will be equal to the distance between the bottom cross-section of the projectile and the cross-section of theprojectile, on which one of the guide belts meets the connecting cone of the barrel, L_{BD} is the length of the bullet chamber. The ductility of the guide belt material is determined by the following parameters: yield limit in tension (compression) σ_τ

, the reinforcement coefficient $\bar{n}$ and the strain hardening coefficient ε_0. The yield limit is the basic mechanical parameter of the belt and depends on the type of material and its strain hardening. The complete strain hardening of the guide belt is formed from the strain hardening of the material when producing the belt billet $\varepsilon_0^{'}$ and the strain hardening of the material when producing the belt $\varepsilon_0^{''}$:

$$\varepsilon_0 = \varepsilon_0^{'} + \varepsilon_0^{''}$$

When pressing the belt into the groove with the diameter d_k can:

- For round workpieces with inner diameter d_t:

$$\varepsilon_0^{''} = 1 - \frac{d_k}{d_t};$$

- For length bar L_t workpieces: $\varepsilon_0^{''} = 1 - \frac{\pi d}{L_t}$

As the hardness increases, the ε_0 hardness yield limit σ_τ increases, i.e. with the additional plastic deformation of the material (ε') an increase in its strength occurs. Assuming that the dependency $\sigma = f(\varepsilon)$ is linear in stages, we find the new value of the yield limit:

$$\sigma_\tau^* = \sigma_{\tau,0}^* + (\frac{d\sigma_\tau^*}{d\varepsilon_0})(\varepsilon - \varepsilon_0)$$

Where ε_0 and ε - relatively full yield and initial deformation;

σ_τ^* - yield limit, corresponding to the initial deformation (hardening).

Given that the complementary deformation ε' relates to the total deformation by the equation.

$$\sigma_\tau^* = \sigma_{\tau,0}^*(1 + \bar{n}\varepsilon^{'})$$

In which: $\bar{n} = \frac{1}{\sigma_\tau^*}(\frac{d\sigma_\tau^*}{d\varepsilon_0})(1 - \varepsilon_0)$ is the strength increase factor of the material.

The geometric parameters of the guide belt are related to its shape and size of the profin,

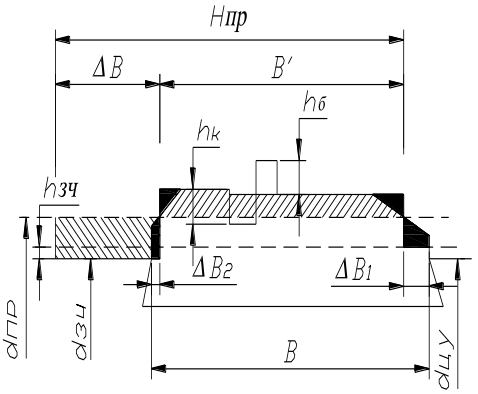

Figure 4. Model of the guide belt profin

In most cases, the profile of the conductor belt is almost rectangular in shape and may have additional parts: the front and rear have inclined sides, winding angles, grooves. The inclined side ensures the best conditions for the start of plastic deformation, holds the projectile, obstructs the movement of the projectile thanks to the sharp increase in the contact surface. The beveled side is in the form of a cone and is characterized by a smaller basic diameter d_{ck}, width (height) B_{ck} and taper angle α_{ck}, $tg\alpha_{ck} = \frac{d_0 - d_{ck}}{B_{ck}}$

The rectangular profile of the glide angle has an inclined side, while the basic dimensions of the glide angle are diameter d_σ, width B_σ, and height h_σ = (d_σ – d_0)/2. The grooves are rectangular in shape and are characterized by the number of grooves n_k, width B_k; bottom diameter d_{kn}, and depth h_k = (d_{kn} – d_0)/2. The width of the profile B (first B_1 and second B_2) serves as the width of the belt that leads to the start of cutting. Include the conversion width of the belt after cutting H_{np} to investigate the belt compression in the plain barrel with the conversion diameter d_{np}, The volume of the pressed material is the same for smooth and grooved barrels. The problem leads to the construction of a new rectangular profile belt of d_{np} size, $d_{зч}$, and H_{np} has an area that needs to be equal to the area of the actual profile. It is more convenient to calculate the inclined side when performing on a graph, switching from the actual width of the belt to the converted width $B' = B - \Delta B_1 - \Delta B_2$ (fig. 4). When calculating the front tilt

side, there can be two cases: $d_{CK} > d_{np}$ và $d_{CK} < d_{np}$ in smooth bore cannons $d_{CK} = d_{np}$.

Knowing the structural characteristics of the projectile system, it is possible to evaluate their influence on the process of cutting the belt leading to the barrel groove and the translational movement of the projectile in the barrel.

3.BUILD A MODEL OF THE GUIDE BELT CUTTING PROCESS OF 23MM TELESCOPIC PROJECTILES

Simulate the number of the guide belt cutting process of the 23mm telescopic warhead to determine the deformation process of the guide belt, the movement of the warhead, the law of belt cutting resistance, the value of the projectile pressure and the law of the pressure of the barrel wall into the guide belt during the belt cutting process. The numerical simulation results are compared and evaluated with theoretical and experimental calculation results.

3.1. Geometric parameters and materials of warheads, guides and barrels

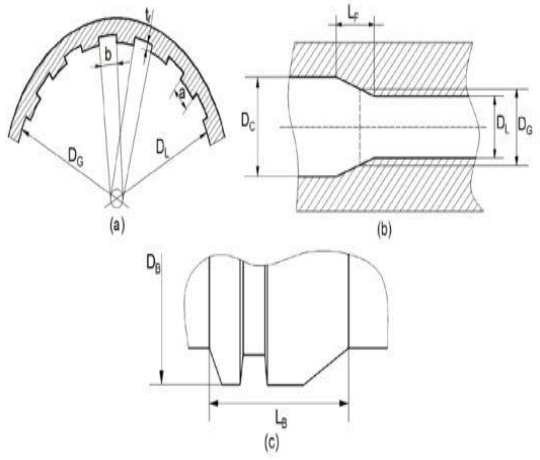

Figure 5. Geometric parameters of the guide belt and gun barrel

The main geometric parameters of the barrel and warhead structure (guide coupling) used for the numerical simulation model are seen in Figure 5 and Table 2. The geometric parameters of the barrel groove, the inlet taper and the size of the guide belt are shown, including: a - the width of the convex ridge of the torsion groove; b - torsion groove width; t - the depth of the barrel groove; D_c - combustion chamber diameter; D_L - diameter of the convex ridge of the torsion groove; D_G - torsion groove diameter; L_f - the length of the inlet of the cannon barrel (including the inlet section without torsion grooves and the inlet section with torsion grooves); D_B - belt diameter; L_B - belt width.

Table 2. Geometric parameters of the belt cutting model (in mm)

a	b	t	D_c	D_L	D_G	L_f	D_B	L_B
3,2	4,0	0,45	32	23	23,9	29	24,1	8,6

3.2. Material parameters according to the Johnson Cook model

Assuming that the barrel and body are absolutely rigid during the belt cutting process, we only pay attention to the parameters: elastic modulus E, poisson coefficient ν and material density ρ. The belt material is selected according to the CU-OFHC2 grade with the parameters according to the documents [20].

Table 3. Johnson Cook Co-Model Material Model Parameters

Specific Volume, ρ	8800		kg/m3	
Coefficient of elasticity, E	11500		MPa	
Coefficient Poisson, ν	0,31			
Johnson Cook Durable Model			**The Johnson Cook demolition model**	
Melting stress of the material, A	206	MPa	D1	0,54
Durability Factor, B	505	MPa	D2	4,89
Effect coefficient of deformation rate, C	0,01		D3	-3,03
Influence coefficient of the degree of distortion, n	0,42		D4	0,014
Effect Coefficient of Temperature, m	1,68		D5	1,12

Melting Point of Material, T_{melt}	1189	K		
Room Temperature, T_{room}				
Reference Distortion Rate, $\dot{\varepsilon}_0$	5.10^{-4}	S-1		

4. NUMERICAL SIMULATION AND RESULT ANALYSIS

4.1. Simulation of the belt cutting process of a 23mm cased telescoped ammunitiont

Step 1: Build a 3D model of the 23mm telescopic warhead and barrel

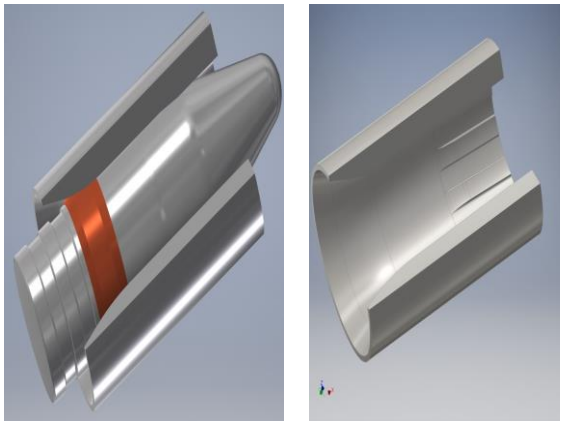

Figure 6. 3D model simulating the cutting process of a 23mm telescopic warhead belt

The parameters of the 23mm telescopic warhead are shown on table 3

Table 3. Parameters of 23mm telescopic warhead

Parameter	Value	Unit
Warhead mass	0,192	Kg
Guide Belt Volume	0,803	Kg

Step 2: Include in the model the material parameters of the guide belt, projectile body, and gun barrel

Step 3: Choose a grid and divide the grid.

The finite element meshing of the model is shown on figure 7.

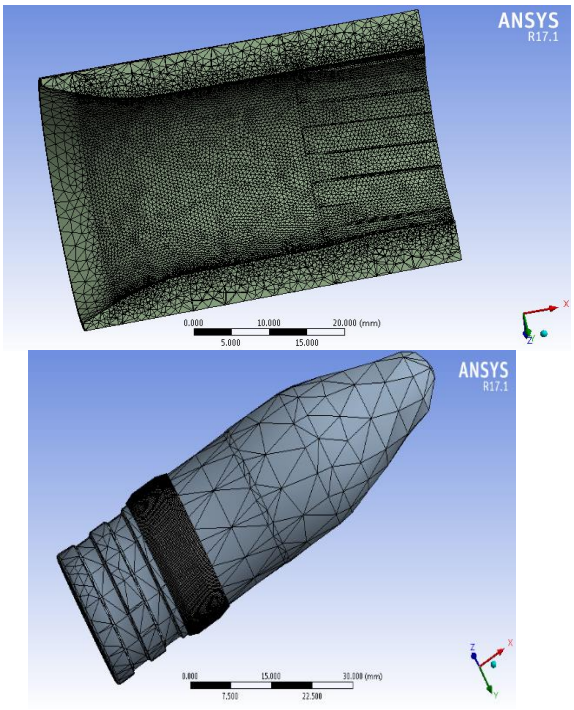

Figure 7. Finite Element Grid

Step 4. Set load conditions, head conditions, and edge conditions.

The time-dependent pressure law of the 23 mm telescopic warhead determined by test firing.

Boundary conditions of the belt-cutting problem:

+ Conditions on the displacement margin: during the belt cutting process, the gun barrel is fixed.

+ Contact margin condition: choose the friction coefficient between the guide belt and the barrel as: 0.1.

Step 5: Solve the problem.

Result:

When solving the problem of simulating the process of cutting the guide belt of the 23mm cased telescoped ammunitiont, we can get the image of the deformation and destruction of the guide belt material during the cutting process, the parameters characteristic of the belt cutting process such as velocity, acceleration, displacement distance of the warhead during the belt cutting process, etc. belt cutting resistance and the value and law of the pressure of the barrel wall on the guide belt, etc.

** Mechanism of 23mm cased telescoped ammunitiont guide belt cutting process*

The deformation morphology of the guide belt during the belt cutting of the 23mm cased telescoped ammunitiont is shown on Figure 8.

Figure 8 shows that during the cutting process, the guide belt is inserted into the barrel groove and pressed between the projectile and the barrel. In the process, the guide belt is lengthened by the tapered face, spine, and bottom of the barrel groove. The cutting grooves on the guide belt are formed by the corresponding barrel groove ridges, the material of the guide belt is stored at the end of the cutting grooves and does not separate the guide belt. Along with that, the material that is stretched and stored at the end of the protruding ridges cut on the guide belt is also easily observed. However, the elongation of the belt material in the parts corresponding to the barrel groove and bottom is completely different.

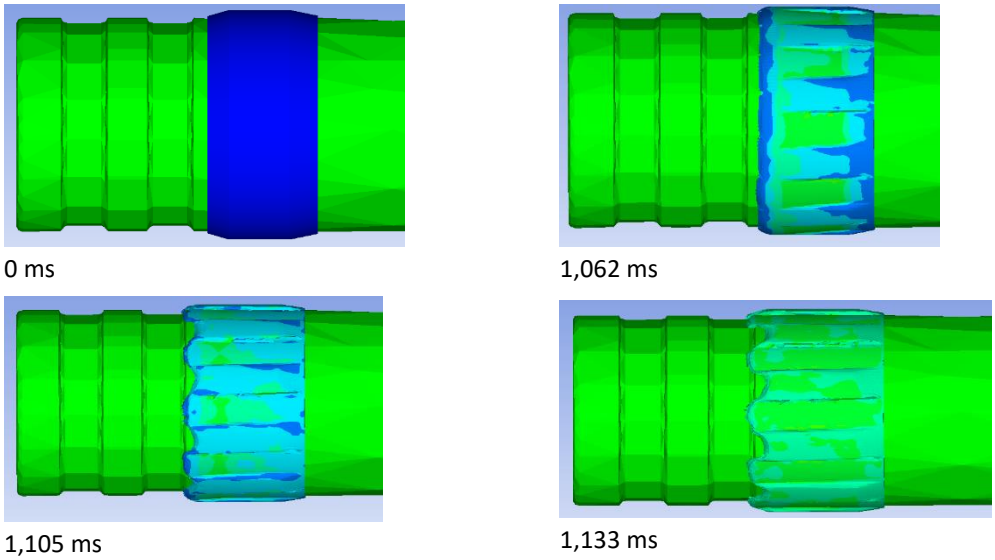

Figure 8. Deformation morphology of the conductor belt

Figure 9 shows the material state during the belt cutting process.. The results obtained clearly indicate that the belt material is completely in a plastic state and there is no destruction of the belt material during the cutting process.

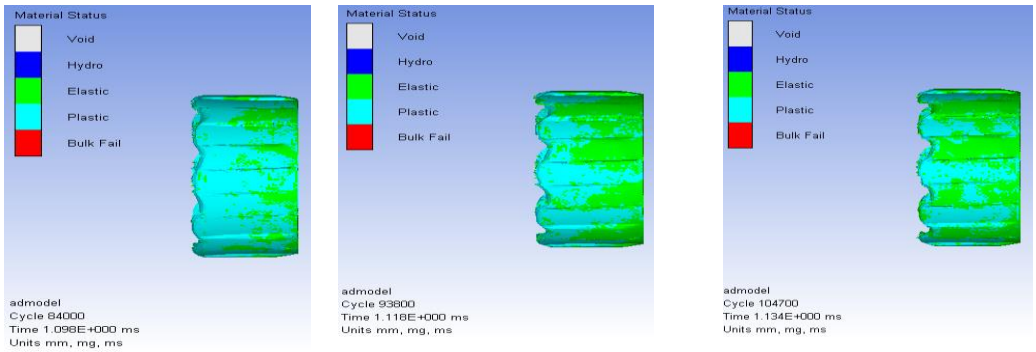

Figure 9. State of of the belt material

4.2. Testing

Images of tests using the MTS Universal Force Generator machine and when testing 23mm cased telescoped ammunitiont.

a. Test warhead by MTS Universal Force b. Warhead after test firing
Generator machine

Figure 10. Warhead and guide belt after test and test firing

The test results show that the deformation morphology of the guide belt after the cutting process is highly similar to the results obtained from numerical simulation. Thus, the digital simulation process has accurately reflected the physical nature of the process of cutting the guide belt of the 23mm cased telescoped ammunitiont.

Measuring and determining the mass of the guide belt after static compression test and numerical simulation found that the mass of the guide belt after the test and numerical simulation did not change, which proved that during the belt cutting process, the guide belt material destruction did not occur. This result is consistent with the results of the material state of the guide belt during the cutting process shown in Figure 10.

The change in the mass of the guide belt during belt cutting: during the belt cutting process, the conductor material is compressed in the diameter direction, the radial-oriented compression displacement of the material is almost linear in the cross-cutting distance x = 24÷25mm, The maximum compression interval ≅ of 0.1mm is achieved when the warhead is displaced by a distance of 24÷25mm, corresponding to the deflection of the guide belt δ = (24.1-23.9)/2 = 0.1 mm (the deflection at the bottom of the barrel groove) and the length of the first entry taper of the barrel structure. After the first entry tape, the radial displacement of the point located on the surface of the guide belt is almost constant (≅ 0.1 mm). The numerical simulation results of the radial compression displacement are in accordance with the initial structural parameters of the guide belt and the barrel of the 23mm cased telescoped ammunitiont.

** Projectile ejection pressure*

According to [3], the shell pressure is determined by the expression:

$$p_0 = \frac{P_{\max}}{S}$$

In which, $P_{\max}$ - maximum cutting resistance; S - cross-sectional area of the warhead.

The shell pressure p_0 depends on the belt structure, which is determined by empirical insertion into the barrel or by numerical simulation (determined by $P_{\max}$ Equation 4). Table 4 shows the p_0 value determined by different methods.

Table 4. Value p_0

TT	Method	Value p_0	Unit
1	Numerical Simulation	144,5	Mpa
2	Lorentz Formula (Лоренца)	88,6	Mpa
3	Snhim formula	42,5	Mpa
4	Gabo formula	62,8	MPa

From the result table, it is found that the calculation results between the methods have a lot of errors, and the numerical simulation results have a greater value than other methods. Therefore, it is necessary to conduct experimental studies on the guide belt model of 23mm cased telescoped ammunitiont for a more accurate assessment.

5. CONCLUSION

This paper has studied an overview of the balistic processes that occur in the firing phenomenon of 23mm cased telescoped ammunitiont. Simulation the belt cutting process of 23mm cased telescoped ammunitiont by using the numerical method. The simulation results provide a visual image of the belt

cutting process, deformation and stress of the belt material. Determine the time of the bullet to completely cut the belt, corresponding to the projectile ejection pressure and the maximum belt cutting force. The simulation results compared to the experimental results have a small error, indicating the accuracy of the presented model.

REFERENCES

[1]. D.Nguyen Thai, D. Nguyen Van, P.Ta Van and L.Do Duc, Biomechanical analysis of the shooter – weapon system oscillation, 2017, *International Conference on Military Technologies (ICMT)*, Brno, 2010, pp.48-53, doi:10.1109/MILTECHS.2017.7988729.

[2]. Zhen Li , Jianli Ge , Guolai Yang , Jun Tang, Modeling and dynamic simulation on engraving process of rotating band into rifled barrel using three different numerical methods, *Journal of Vibroengineering*, Vol. 18, Issue 2, 2016, p. 768-780.

[3]. Qian L F, Hou B L and Xu Y D 2016, Gun ballistics (Beijing: *Beijing Institute of Technology Press*) pp150-151.

[4]. Li M, Qian L F and Sun H Y 2016, Research on coupled thermo-mechanical model during rotating band engraving process, *J. Acta Armamentarii* **37(10)** 1803-1811.

[5]. Zhang H and Zhou Y H 2006, Research on the Engraving Process of CTA, *J. Journal of Ballistics* **18(1)** 76-79.

[6]. Keinänen H, Moilanen S, Tervokoski J, et al 2012, Influence of Rotating Band Construction on Gun Tube Loading-Part I: Numerical Approach *J. Journal of Pressure Vessel Technology* **134** 041007-1.

[7]. Toivola J, Moilanen S, Tervokoski J, et al 2012, Influence of Rotating Band Construction on Gun Tube Loading-Part II: Measurement and Analysis *J. Journal of Pressure Vessel Technology* **134** 041006-1.

[8]. Ma M D, Cui W S, Zeng Z Y, et al 2015, Engraving process analysis of projectiles based on coupling of FEM and SPH *J. Journal of Vibration and shock* **34(6)** 146-150.

[9]. Lu Y, Zhou K D, He L, et al 2014, Numerical simulation and analysis of engraving duration interior ballistics of some large-caliber small arms *J. Journal of Ballistics* **26(2)** 67-71.

[10]. Ding C J, Zhang X Y 2015, Simulation study of bearing band engraving process and interior ballistic process based on thermo-mechanical coupling FEA model, *J. Aeta Armamentarii* **36(12)** 2254-2261.

[11]. Ding L, Jiang J W, Men J B and Wang S Y 2021, Numerical simulation of the fracture characteristics of copper EFP with different constitutive models *J. Journal of Physics: Conference Series* **1813(1)** 012012.

[12]. Wu B, Zheng J, Tian Q, et al 2014, Friction and wear between rotating band and gun barrel during engraving process, *J. Wear* **318** 106-113.

[13]. Wu B, Fang L H, Zheng J, et al 2019, Stain hardening and strain-rate effect in friction between projectile and barrel during engraving process, *J. Tribology Letters* **67(39)** 38-45.

[14]. Sun Q Z, Yang G L, Wang P, et al 2015, Numerical Research on Rotating Band Engraving process of a large-caliber howitzer *J. Acta Armamentraii* **36(2)** 206-213.

[15]. Shen C, Zhou K D, Lu Y, et al 2018, Research on the influence of damaged bore of a large caliber machine gun on bullet engraving progress *J. Acta Armamentarii* **39(12)** 2320-2329.

[16]. Zou L B, Yu C G, Feng G B, et al 2021, Friction Model of Projectile Engraving Process Based on Temperature Correction *J. Acta Armamentarii* **42(6)** 1148-1156.

[17]. Qian L F and Chen G S 2020, Firing accuracy theory of medium and long range suppressed artillery, (Beijing: *Science Press*) p329.

[18]. Zhou Y H and Wang S C 1990, Practical two-phase flow interior ballistics (Beijing: *Publishing House of Ordnance Industry*).

[19]. Johnson G R and Cook W H 1985, Fracture characteristics of three metals subjected to various strains, strain rates, temperatures and pressures *J. Engineering Fractures Mechanics* **21(1)** 31-48.